The impact of weakly bound 89Zr on preclinical studies: Non-specific accumulation in solid tumors and aspergillus infection

Severin, Gregory; Jørgensen, Jesper T.; Wiehr, Stefan ; Rolle, Anna-Maria ; Hansen, Anders Elias; Maurer, Andreas ; Hasenberg, Mike ; Pichler, Bernd ; Kjær, Andreas; Jensen, Andreas Tue Ingemann

Published in:
Nuclear Medicine and Biology

Link to article, DOI:
10.1016/j.nucmedbio.2014.11.005

Publication date:
2015

Document Version
Peer reviewed version

The impact of weakly bound ^{89}Zr on preclinical studies: Non-specific accumulation in solid tumors and aspergillus infection

Gregory W Severin[1,4], Jesper T Jørgensen[2], Stefan Wiehr[3], Anna-Maria Rolle[3], Anders E Hansen[2,4,5], Andreas Maurer[3], Mike Hasenberg[6], Bernd Pichler[3], Andreas Kjær[2], and Andreas I Jensen*[1,4]

[1] *The Hevesy Laboratory, DTU Nutech, Technical University of Denmark*

[2] *Dept. of Clinical Physiology, Nuclear Medicine & PET, Rigshospitalet and Cluster for Molecular Imaging, Faculty of Health Science, University of Copenhagen, Denmark*

[3] *Werner Siemens Imaging Center, Department for Preclinical Imaging and Radiopharmacy, Eberhard Karls University Tübingen, Tübingen, Germany*

[4] *Center for Nanomedicine and Theranostics, Technical University of Denmark*

[5] *Department of Micro- and Nanotechnology, DTU Nanotech, Technical University of Denmark*

[6] *University Duisburg-Essen, University Hospital, Institute for Experimental Immunology and Imaging, Essen, Germany;*

* Corresponding author: Technical University of Denmark, Frederiksborgvej 399, bld. 202, 4000 Roskilde, Denmark. Tel: +45 20126187; Fax: +45 46775347.

E-mail address: atije@dtu.dk (A. Jensen)

Abbreviated title: ^{89}Zr accumulation in tumors and aspergillosis

Key words: Zr-89, PET/MR, mouse model, cancer, infection, Aspergillus fumigatus

Abstract

Preclinical studies involving ^{89}Zr often report significant bone accumulation, which is associated with dissociation of the radiometal from the tracer. However, experiments determining the uptake of unbound ^{89}Zr in disease models are not performed as routine controls. The purpose of the present study was to investigate the impact of free or weakly bound ^{89}Zr on PET quantifications in disease models, in order to determine if such control experiments are warranted. **Methods:** Chemical studies were carried out to find a ^{89}Zr compound that would solubilize the ^{89}Zr as a weak chelate, thus mimicking free or weakly bound ^{89}Zr released in circulation. ^{89}Zr oxalate had the desired characteristics, and was injected into mice bearing FaDu and HT29 solid tumor xenografts, and mice infected in the lungs with the mold *Aspergillus fumigatus*, as well as in healthy controls (naïve). PET/CT and PET/MR imaging followed to quantify the distribution of the radionuclide in the disease models. **Results:** ^{89}Zr oxalate was found to have a plasma half-life of 5.1 ± 2.3 h, accumulating mainly in the bones of all animals. Both tumor types accumulated ^{89}Zr on the order of 2-4% ID/cm^3, which is comparable to EPR-mediated accumulation of certain species. In the aspergillosis model, the concentration of ^{89}Zr in lung tissue of the naïve animals was 6.0 ± 1.1 %ID/g. This was significantly different from that of the animals with advanced disease, showing 11.6% ± 1.8 %ID/g. **Conclusions:** Given the high levels of ^{89}Zr accumulation in the disease sites in the present study, we recommend control experiments mapping the biodistribution of free ^{89}Zr in any preclinical study employing ^{89}Zr where bone uptake is observed. Aqueous ^{89}Zr oxalate appears to be a suitable compound for such studies. This is especially relevant in studies where the tracer accumulation is based upon passive targeting, such as EPR.

1. Introduction

^{89}Zr is a popular radionuclide for the radiolabeling of monoclonal antibodies (mAbs) and similar proteins for PET imaging [1–5]. However, several studies on ^{89}Zr-radiolabeled mAbs show significant bone uptake of ^{89}Zr [2,6,7]. This uptake is often attributed to chelate instability, with ^{89}Zr being released during the long circulation time of the mAb [2]. Alternatively, Holland et al. suggested a metabolic process [8]. Regardless of the cause, the accumulation of radioactivity in bones is indicative of ^{89}Zr that is no longer bound to the tracer. The presence of this unbound ^{89}Zr during a PET scan can potentially have a large impact on the interpretation of results, especially if it is accumulating at the disease site. In current practice however, appropriate control experiments are not reported.

The biodistribution of free, or weakly chelated, ^{89}Zr was investigated in healthy mice by Abou et al. using the chloride, oxalate, phosphate and citrate salts [9]. All salts were found to exhibit similar biodistribution and cause accumulation of ^{89}Zr in the bones, except the phosphate, which localized to liver and spleen. This was attributed to poor solubility of the ^{89}Zr phosphate. Holland et al. also found the activity from the ^{89}Zr oxalate to show pronounced bone accumulation, but found ^{89}Zr injected as the chloride to accumulate in the liver [8]. This was also attributed to the chloride being prone to hydrolysis and poor solubility. These studies both indicated that free, soluble $^{89}Zr^{4+}$ will accumulate in bone.

The nonspecific biodistribution of free ^{89}Zr in clinically relevant disease models has not been investigated. However, given the large number of reports showing increased bone uptake in monoclonal antibody imaging, which indicates the presence of free ^{89}Zr, knowledge of the distribution of free ^{89}Zr in animal models of human disease is important. In tumors, the accumulation of naked or weakly chelated radiometals, such as ^{67}Ga [10], and ^{64}Cu [11], is well established. For this reason, ^{67}Ga salts have a long history of use in tumor imaging. ^{67}Ga distributes via binding to transferrin [10], and it is reasonable to suspect that the same pathway might be available for Zr^{4+}, or ZrO^{2+} [12]. Accordingly, free ^{89}Zr could show nonspecific tumor accumulation through this pathway, which might disturb the correct interpretation of accumulation data from mAb imaging. In addition, enhanced permeation and retention (EPR) dominated localization after metal association with endogenous serum proteins, such as albumin, may give rise to lesion uptake of free ^{89}Zr [13,14]. As nanoparticles are typically thought to localize to tumors via EPR [15], the presence of free ^{89}Zr may have consequences for the interpretation of tumor accumulation data for ^{89}Zr-labeled nanoparticles.

^{89}Zr-labeled antibodies are not only in use for tumor imaging, but are also being investigated for the diagnosis of other diseases such as pulmonary aspergillosis. In *Aspergillus fumigatus* infections, an extracellular siderophore is excreted by the mold [16]. This was recently utilized by Petrik et al. in preclinical PET studies with ^{68}Ga labeled siderophores TAFC and FSC [17,18]. These chelators exhibit multiple hydroxamate groups, similar to the most successful ^{89}Zr chelator desferrioxamine B, which itself is a siderophore produced by streptomyces bacteria [19]. Such extracellular siderophores may take up free or weakly bound ^{89}Zr and facilitate its

accumulation in *Aspergillus* infected tissues. This accumulation, coupled with the EPR-mediated accumulation occurring as a result of inflammation and transferrin-receptor upregulation, could give a very significant PET signal from lung accumulation of free or weakly bound ^{89}Zr in circulation in pulmonary aspergillosis. Therefore, knowledge of the biodistribution of free ^{89}Zr in solid tumors as well as in other disease sites, such as *A. fumigatus* infected tissues, is crucial before initiating a preclinical positron emission tomography (PET) study with ^{89}Zr.

The aim of this work was to investigate the biodistribution of weakly chelated ^{89}Zr in relevant murine disease models compared to their healthy controls. We set out to determine whether 1) free ^{89}Zr exhibits accumulation in FaDu and HT29 tumor xenografts in mice and 2) whether biodistribution, especially in lungs, is significantly different between healthy animals and those with pulmonary aspergillosis. Further, the criteria for the injected ^{89}Zr to be considered 'free', was that it was stable in solution and able to interact and associate with complexing molecules and other blood stream components. For this reason we also investigated a range of complexing ligands for their ability to restrict hydrolysis of ^{89}Zr and allow chelation by *diethylene triamine pentaacetic acid* (DTPA).

2. Materials and Methods

2.1. Materials

Yttrium foils were purchased from Alfa Aesar. All solvents and chemicals were purchased from Sigma Aldrich. ^{89}Zr was produced on a GE PETtrace Cyclotron. Radio-TLC was performed on a Raytest MiniGita Star. All TLC analyses were performed on silica gel 60 F_{254} plates (Merck) with 5% (w/v) NH_4OAc in H_2O-MeOH (1:1) as eluent, in which the R_f of ^{89}Zr-DTPA is 0.7 and $^{89}Zr^{4+}$ does not elute. Radioactivity was measured using a Veenstra Instruments dose calibrator VDC-505. QMA cartridges were from Waters. Osmolalities were measured on an Osmomat 030 cryoscopic osmometer (Gonotec). pH was measured on an Inolab 740 electronic pH-meter (WTW). Radionuclidic purity was measured on an LGC-5 high purity germanium detector (Princeton Gamma-Tech). Metal ions were quantified with an ICAP 7000 ICP-OES (Thermo Scientific). Ultrapure water was used in all cases (Milli-Q water purification system, Millipore).

^{89}Zr chloride was prepared according to the method of Holland *et al.* [20]. In brief, natural 660 µm thick yttrium foils, were irradiated with 15 µA of protons degraded from 16 MeV to 11 MeV with an 800 µm aluminum plate. The produced $^{89}Zr^{4+}$ was separated from the yttrium target after digestion in aqueous HCl (3 mL, 6 M) by trapping on hydroxamate resin (50-100 mg), followed by elution of the $^{89}Zr^{4+}$ in aqueous oxalic acid (3 mL, 1 M). A quarternary methyl ammonium Sep-Pak cartridge (QMA light, Waters) was used to trap the anionic ^{89}Zr oxalate complex from the oxalic acid solution, and after washing with ultrapure water (30 mL), the ^{89}Zr

was released in aqueous HCl (200 µL, 2 M). This solution was taken to dryness under argon flow at 110 °C for 15 minutes, furnishing ^{89}Zr chloride.

2.2. Comparison of aqueous solutions for injection of 'free' ^{89}Zr

The following experiments were performed to test the ability of various complexing ligands to restrict hydrolysis of ^{89}Zr and allow chelation by DTPA. To vials containing dry ^{89}Zr chloride was added 1.3 mL of either 1) saline, 2) 10 mM oxalic acid in saline at pH ≈ 5.5, 3) 10 mM oxalic acid in saline at pH ≈ 7.0, 4) 10 mM citric acid in saline at pH 5.5, 5) 10 mM citric acid in saline at pH 7.0, 6) neat ultrapure water, 7) isotonic sucrose solution at 924 mg/mL, 8) 10 mM sodium acetate at pH 5.5 or 9) 10 mM sodium acetate at pH ≈ 7.0. Each preparation was stirred for 10 minutes at 37 °C after which 300 µL was removed for pH measurement. In addition, the radioactivity in the total volume (1.3 mL) as well as in the removed 300 µL was measured. To the remaining 1.00 mL was then added aqueous DTPA (50 µL, 50 mM) that had been adjusted to pH 5.5 or pH 7.0, whichever was closest to the pH of the receiving ^{89}Zr-mixture. To the saline (chloride), water and sucrose mixtures was added DTPA at pH 5.5. The solutions were then stirred at 37 °C and monitored by radio-TLC with samples removed at t = 0 (before addition of DTPA), t = 10 min, t = 30 min and t = 60 min. Each mixture was prepared and analyzed in triplicate.

2.3 Preparation and characterization of the ^{89}Zr oxalate for in vivo use

Based on the stability and exchange experiments described above, an oxalate solution was chosen for *in vivo* use. This was prepared by adding a solution of 10 mM oxalic acid in isotonic

saline (pH adjusted to 6.7 with NaOH) to the dried ^{89}Zr chloride. In order to confirm that the ^{89}Zr was fully dissolved, a sample of the solution was removed and its activity concentration was compared to the remaining fraction. Osmolality and pH were measured, and HPGE gamma spectroscopy was used to determine the radionuclidic purity. ICP-OES, calibrated against Fe, Zr, Zn, Cu, Ag, and Ni standards in 1% (w/v) HCl, was used to quantify metal impurities. Additionally, 300 µl of the ^{89}Zr oxalate solution was removed and mixed with aqueous DTPA (15 µL, 50mM, pH 7.0). After stirring at 37 ^{o}C for 30 min, it was analyzed by radio-TLC along with a sample to which no DTPA had been added. After the completion of these tests, the solution was ready for injection in the animal studies.

2.4 In vivo studies on tumor-bearing mice

The studies on tumor-bearing mice were approved by the Danish Animal Welfare Council, Ministry of Justice. Human head and neck cancer cell line, FaDu and human colorectal cancer cell line, HT29 (purchased from ATCC) were cultured in MEM medium with Earle's salts and McCoy's 5A medium, respectively (both from Sigma-Aldrich); with 10% fetal calf serum, and 100 units/mL penicillin and 100 µg/mL streptomycin (Invitrogen) at 37 °C in 5% CO_2. In addition the MEM medium was supplemented with 1% MEM non-essential amino acids solution (100x), 1 mM sodium pyruvate (both from Invitrogen) and 2 mM L-glutamine (Sigma-Aldrich). Tumors were established in the left and right flank of seven-week old female NMRI nude mice (Taconic Europe) by subcutaneous injection of 10^6 cancer cells dissolved in 200 µL of a 1:1 mixture of Matrigel^{TM} (BD-Biosciences) and growth medium and were allowed to grow for 2-3 weeks for tumor volumes of 50-500 mm^3. Animals had access to chow and water ad libitum. For tracer

administration and during scans, the mice were placed in a nose cone and breathed gas anesthesia (2.5% Sevoflorane (Abbot Scandinavia) mixed with 35% O_2 in N_2). A heating pad was used to keep the body temperature stable. ^{89}Zr oxalate solution (100 µL, 9-15 MBq) was injected into the tail vein of mice bearing FaDu (n = 3) and HT29 tumor xenografts (n = 4). Ten minute static scans were performed on a small animal PET scanner (microPET 120, Siemens Medical Solutions) at 1 h, 6 h, 20 h, 45 h, and 68 h post injection with an energy window 350-650 keV and 6 ns time resolution. Each PET scan was followed by seven minutes small animal CT scans (MicroCAT II Tomograph; Siemens Medical Solutions) with tube voltage and tube current set at 70 kVp and 500 µA, respectively and an exposure time of 310 ms per projection (360°; 360 projections). Listmode data from PET acquisitions were post-processed into sinograms and reconstructed using the maximum a posteriori (MAP) algorithm. Images had a resolution of 1.2 mm at the center field of view. PET and CT images were fused using Inveon software (Siemens Medical Solutions), ROIs were drawn on different target tissue and uptake quantified as % injected dose per cubic centimeter (%ID/cm^3). Additionally, the tumor-to-muscle (T/M) and tumor-to-blood (T/B) ratios were calculated. From the images it was evident that the myocardium did not accumulate high levels of ^{89}Zr oxalate. As it is impossible to delineate the left ventricle of the mice based on CT scans without contrast, a ROI created on the heart was used for T/B-ratio and blood-circulation half-life calculations.

2.5 In vivo studies on A. fumigatus infected and naïve mice

The studies on *A. fumigatus* infected and disease-free control mice ("naïve") were performed according to the German Animal Protection Law with permission from the responsible local

192 authorities. Infections were performed as described by Bruns *et al* [21]. Briefly, eight-week old
193 female C57BL/6 mice (Harlan Laboratories) were rendered neutropenic by an intraperitoneal
194 injection of 100 µL anti-Gr-1 antibody solution (clone RB6-8C5 at a concentration of 1 mg/mL,
195 BioXCell). 24 h later a pulmonary *A. fumigatus* infection was induced by an intratracheal
196 application of $4x10^6$ resting *A. fumigatus* spores (strain ATCC 46645), suspended in 100 µL
197 sterile tap water. For this step the animals were anaesthetized by an intraperitoneal injection of
198 100 µL Ketamin/Rompun solution (Ketamin: 80 mg/kg, Ratiopharm GmbH, Ulm, Germany;
199 Rompun: 15 mg/kg, Bayer HealthCare, Leverkusen, Germany). After reaching deep narcosis, the
200 animals were intubated using a 22G indwelling venous catheter (Vasofix Braunüle, B. Braun AG,
201 Melsungen, Germany) and subsequently the spore suspension was applied. To achieve a better
202 distribution of the spore mass and to avoid suffocation the animals were ventilated for one
203 minute with a small animal respirator (MiniVent, Hugo Sachs, March-Hugstetten, Germany) at a
204 rate of 250 breaths per minute at an inhalation volume of 300 µL per breath. Animals had
205 access to food and water ad libitum.
206
207 ^{89}Zr oxalate solution (50 µL, 10-12 MBq), was injected via the lateral tail vein. During imaging,
208 the animals were anesthetized with 1.5% isoflurane mixed with 100% oxygen. Anesthesia was
209 monitored by measuring the respiratory frequency, and the body temperature was kept at 37°C
210 by a heating pad. All mice were imaged using a small animal PET scanner (Inveon, Siemens
211 Preclinical Solutions), yielding a spatial resolution of approximately 1.3 mm. PET data were
212 acquired in list-mode, histogrammed in one 10 min time frame for the static scans and
213 reconstructed using an iterative ordered subset expectation maximization (OSEM) algorithm.

No attenuation correction was applied. Magnetic resonance (MR) imaging was performed on a 7 T small animal MR tomograph (Clinscan, Bruker Biospin MRI) obtaining anatomical information for optimized organ delineation. A T2-weighted 3D space sequence (TE / TR 202 / 2500 ms, image matrix of 137 x 320, slice thickness 0.27 mm) was used for whole-body imaging. PET images were normalized to each other, subsequently fused to the respective MR images and analyzed using Inveon Research Workplace software (Siemens Preclinical Solutions). Results are expressed as percentage of the injected dose per cm^3 (%ID/cm^3). After the last PET scan, the animals were sacrificed by cervical dislocation under deep anesthesia and dissected. Organs were removed, weighed and measured with an aliquot of injected solution in the γ-counter (Wizard single-detector γ-counter; Perkin Elmer) using an energy window between 350 and 650 keV.

The *A. fumigatus* infected mice were divided into two different groups. The first group (n = 5), termed “nascent disease”, received the tracer injection immediately after infection. These animals, along with neutropenic uninfected controls (n = 5), “naïve”, mice were imaged with 10 min PET scans, followed by MR imaging, performed at 3, 24 and 48 h post-injection of the tracers. In the second group (n = 4), termed “advanced disease”, infected mice were injected with ^{89}Zr oxalate 21 hours after infection. This cohort, along with four naïve control animals, was imaged 3 h after tracer injection, followed immediately by *ex vivo* biodistribution.

2.6 Statistical Analysis

Statistical analysis was performed using a two-tailed t-test. Data were considered statistically significant for $p < 0.05$. All quantitative results are shown as the mean $\pm$ 1 standard deviation (SD).

3. Results

3.1 Comparison of aqueous solutions for injection of 'free' ^{89}Zr

The results from the tests on the various ^{89}Zr-mixtures are presented in **table 1** (pH values for the mixtures) and **figures 1A** (transferability/dissolution) and **1B** (transchelation to DTPA). For the pH measurements in general, the solutions with low buffer capacity at their respective pH values became slightly more acidic after mixing with the dried ^{89}Zr activity. This was likely due to leftover oxalic acid residue from the chemical separation. Our lowest water pH measurement was pH = 4.65, which indicates that oxalic acid concentration was less than 13 µM (see **supplemental materials** for calculation). According to the work of Kobayashi *et al.* [22], Zr^{4+} is present as the insoluble hydroxide complex at such low oxalate concentrations. This was reflected by our transferability tests (**figure 1A**). In solutions with an efficient complexing agent in sufficient concentration to restrict hydrolysis, such as oxalate, citrate, or sucrose, ^{89}Zr was readily taken into the aqueous phase, whereas hydrolysis-prone mixtures, such as water, acetate, and chloride, resulted in incomplete dissolution of the ^{89}Zr.

Despite the fact that several solutions were able to bring ^{89}Zr into the aqueous environment, it remained necessary to test whether the ^{89}Zr was still able to transchelate to DTPA. This would ensure that the ^{89}Zr was not merely suspended as a colloid, and that the complexes in question could easily transfer the radioactivity to other agents. All complexes were tested for transchelation to DTPA, but only the ones with superior transferability are shown in **figure 1B**. For the remainder, please refer to **supplemental materials**. Both oxalate mixtures showed fast

and efficient transchelation to DTPA, within 10 minutes. On the other hand, the uptake from the citrate was markedly slower, showing a gradual ascent, reaching about 70-80% after one hour. DTPA chelation from the sucrose was faster than from the citrate, but slower than from the oxalate.

Based on the results described above, we decided to use the oxalate complex for *in vivo* studies, while keeping the pH below 7. The main reason for choosing oxalate over citrate was that we desired a complex with a higher propensity for transferring ^{89}Zr to other chelating agents present in serum. This was expected to prevent fast renal clearance of the charged complexes and to better mirror the *in vivo* situation where weakly bound ^{89}Zr is released and presumably bound to endogenous serum components.

3.2 Preparation and characterization of the ^{89}Zr oxalate solution for in vivo use

The results of the quality control analyses for the injected ^{89}Zr oxalate solutions were consistent with those observed in the transferability/solubility and transchelation tests described above. The transferability of activity in the ^{89}Zr oxalate *in vivo* formulation was 95%, indicating that the ^{89}Zr was properly dissolved. The pH value was in the range of 5.5-6.7, which due to the low buffer capacity of the solution was expected to fluctuate. The osmolality was 310 mOsmol/kg, and was appropriate for injection (serum osmolality: 282 - 295 mOsmol/kg). Analysis by ICP-OES showed both non-radioactive Zr and Fe to each be present in concentrations on the order of 200 ppb. This gave specific activities against total Zr and Fe of 20-35 GBq/µmol at time of injection. Analysis by gamma spectroscopy showed only peaks originating from ^{89}Zr, indicating

radionuclidic purity over 99%. Analysis of the ^{89}Zr oxalate solution by radio-TLC showed that >99% of the activity stayed at the origin. Following addition of DTPA, 98% of the activity shifted to the Zr-DTPA peak after 30 minutes (93% after 10 minutes). This confirmed a radiochemical purity of >95%, and that the activity was freely transchelated from the oxalate complex to other chemical species.

3.3 In vivo data from tumor-bearing mice

Representative PET/CT images from the FaDu and HT29 tumor-bearing animals are given in **Figure 2**, with organs denoted. Tumor contrast is clearly seen at both 1 h and 45 h. However, 45 h images are dominated by high bone accumulation.

Quantifications of the PET data are given in **Table 2**. Both tumor types showed significant uptake of 2-4% ID/cm^3 over the course of the study. As expected, bone uptake was prominent, reaching a maximum at 20 h, followed by a plateau at around 13% ID/cm^3. The tumor-to-muscle (T/M) and tumor-to-blood (T/B) ratios in each tumor model are displayed in **Figure 3**. The T/M values ranged from 1.5-3.7 at all time-points, reflecting the contrast observed in **Figure 2.** The long circulation time of the ^{89}Zr oxalate is evident in the heart ROI data. To obtain the clearance half-life, the heart ROI time activity curve for each animal was fitted with an exponential function (unweighted least squares fit with constant background). The average (± 1 SD) blood clearance half-life was 5.1 ± 2.3 h (n = 7) (refer to **supplemental materials** for calculation).

3.4 In vivo data from Aspergillus-infected mice and healthy controls

The mice infected with *A. fumigatus* were divided into two groups. In the nascent disease group, where animals received the tracer injection immediately after they had been infected, and their naïve controls, the PET and biodistribution data were independent of disease status (**Figure 4A-D**). Quantification of the PET results revealed enhanced uptake of ^{89}Zr in the spine (**Figure 4C**) without significant differences between the tested groups. The bone uptake pattern is evident by qualitative observation in the 48 h maximum intensity projection (MIP) images in **Figure 4E**. The mean tracer uptake in the spine of naïve mice increased from 7.5 $\pm$ 0.9 %ID/cm^3 at 3 h to 18.6 $\pm$ 1.0% ID/cm^3 at 24 h, and in infected animals from 7.5 $\pm$ 0.3 % ID/cm^3 at 3 h to 16.5 $\pm$ 1.6 % ID/cm^3 at 24 h after tracer injection, further reflecting the similarity between infected and naïve animals.

Contrastingly, for the group of animals with advanced disease, those infected with *A. fumigatus* 21 hours prior to tracer injection, the biodistributions were markedly different from the healthy controls. Static PET images at 3 hours post injection **(Figure 5)** revealed significantly higher uptake of ^{89}Zr (7.8 ± 1.3 %ID/cm^3) in the lungs of *A. fumigatus* infected animals compared to the naïve group (5.7 ± 0.3 %ID/ cm^3; p = 0.048, **Figure 6**) In addition, the uptake of ^{89}Zr in the spine of naïve animals was significantly higher (6.5 ± 0.7 %ID/cm^3) compared to the infected group (4.8 ± 0.3 %ID/cm^3; p = 0.0088, **Figure 6**). No significant differences were seen in liver and muscle tissues (**Figure 6**).

The *ex vivo* biodistribution from the advanced disease group confirmed the quantification obtained from the PET imaging (**Table 3**). The data from all animals revealed high concentrations of ^{89}Zr in the bones, blood, and highly blood-perfused organs such as the heart. The %ID/g values of the blood were 10.5 ± 2.7 (naïve animals) and 8.6 ± 2.8 (advanced disease). The *ex vivo* biodistribution confirmed the significant differences in the lung ($p = 0.002$) and spine ($p = 0.045$) uptake between the infected and naïve animals observed with *in vivo* PET quantification.

4 Discussion

^{89}Zr has a half-life of 3.27 days and is therefore a useful radionuclide for elucidating the biodistribution of long-circulating, biologically relevant molecules, such as antibodies and nanoparticles. Currently, it is one of the most widely used nuclides for PET imaging at time-points beyond two days post-injection. It allows researchers to understand how a labeled molecule distributes, giving useful information that leads to better drug and tracer development.

The weakness in the current practice is that the derived images quantify the distribution of the radionuclide and not necessarily the intact tracer. In general this is a well-understood phenomenon in PET that can be controlled for by metabolite analysis. However, in ^{89}Zr imaging the problem is rarely addressed. This is surprising because in a large number of pre-clinical studies involving ^{89}Zr there is heightened bone accumulation in the animals. Such high skeletal uptake is indicative of ^{89}Zr that is no longer bound to the molecule of interest, but is free or weakly coordinated. Given that there is an observed separation between radionuclide and the traced molecule, it is important to understand how the free radionuclide is affecting the PET data.

In PET imaging of antibodies ^{89}Zr is usually located in the desferrioxamine (Df) chelator. Within Df, it is present as $^{89}Zr^{4+}$, with water taking up the remaining coordination sites rather than =O or –OH [8]. This incomplete occupation of the first coordination shell by Df has been pointed to

as a chink in the armor of an otherwise incredibly stable chelate, and a possible cause for release of free ^{89}Zr in preclinical studies [23]. Another reason for the presence of free ^{89}Zr in mAb studies is non-specific binding of the radiometal to the protein. Often, radiolabeling is reported with less than 100% yield [6,7], which means either that Df-chelation sites were in shortage or that the reaction had not run to completion. In such cases surplus ^{89}Zr will be present in the reaction mixture and it is reasonable to assume that some of it could bind non-specifically to certain proteins. Finally, it is possible that free ^{89}Zr arises from metabolism of the radiolabeled entities.

Regardless of the mechanism by which ^{89}Zr is released to the circulation, we sought a tracer that would solubilize and efficiently disperse the ^{89}Zr while restricting irreversible hydrolysis. We found that a solution of the radioactivity in 10 mM oxalate in isotonic saline with a pH of 5.0-6.5 adequately provided the desired properties. This was shown by the high solubility of the ^{89}Zr in the mixture and its rapid chelation by DTPA. In addition, the *in vivo* results showed limited liver accumulation. This is consistent with results reported by Abou et al. and by Holland et al. where ^{89}Zr oxalate was not accumulating in the liver of healthy animals [8,9]. On this basis, we conclude that our injected ^{89}Zr was adequately dissolved. Also, the plasma half-life of our injected activity was 5.1 ± 2.3 h. Usually, small molecular, exogenous, highly charged species, such as ^{89}Zr oxalate, can be expected to undergo fast renal clearance, as is the case with free ^{89}Zr-Df [8]. For this very reason, the short circulation time of ^{89}Zr-Df makes it unsuited as a tracer for monitoring the biodistribution of weakly bound ^{89}Zr. That the injected radioactivity in our studies showed prolonged retention in blood suggests that either the

activity is shifted to other endogenous carriers with long circulation, or that the ^{89}Zr oxalate itself is long-circulating. In both cases, since the oxalate is a weak complex, the long circulatory property of the activity is beneficial to its distribution *via* the routes that could be expected of ^{89}Zr weakly bound to long-circulating species, such as antibodies or nanoparticles.

Our initial screening of ^{89}Zr formulations revealed chloride (as saline) to inadequately prevent hydrolysis and keep ^{89}Zr in solution, for which reason we deemed it unfit for *in vivo* use without an additional complexing ion. This agreed with the studies performed by Holland et al., where the chloride formulation was found to exhibit heavy liver accumulation [8]. In contrast, Abou et al. found the chloride (as saline) to distribute similarly to otherwise free ^{89}Zr, with activity mainly localizing to bones [9]. Accordingly, there is a discrepancy between the results of these groups with regards to the chloride. Our study primarily supports the results for the chloride achieved by Holland et al. It is possible that traces of oxalic acid remaining after preparation of the chloride could aid in the solubilization and unrestricted biodistribution of ^{89}Zr present in an otherwise chloride containing mixture. It should be noted that we employed the same method for preparing the ^{89}Zr chloride as Holland et al., and therefore we could be expected to observe the same insolubility [8].

^{89}Zr that is released *in vivo* has the opportunity of being taken up by endogenous binding agents. Likely candidates for such binding include transferrin (Tf) and albumin. Transferrin labeled with ^{89}Zr through Df has been shown to accumulate in tumors and inflammations, due to the upregulation of transferrin receptors as part of an inflammatory response [24,25].

However, binding of ^{89}Zr to the endogenous ferric binding site of transferrin without the use of a chelator was found to be less suitable for *in vivo* use by Holland *et al*. [24]. The conclusion that endogenous labeling was not viable as a method for producing stable ^{89}Zr-Tf for *in vivo* imaging does not exclude the possibility of *in vivo* ^{89}Zr transport via transferrin. The somewhat analogous labeling of transferrin by ^{45}Ti, and its subsequent reported localization to tumors, indicates that tumor accumulation of hard, oxophilic radiometals can be due to binding to transferrin [26]. The results from the HT29 and FaDu tumor models presented here do not show the striking contrast (14.9 %ID/cm^3 tumor accumulation at 24 h) observed by Vavere *et al*. for ^{45}Ti-transferrin; albeit the difference could be attributed to the different affinities of transferrin toward the metals. However, the range of the tumor accumulations we observed are consistent with uptake based upon EPR, such as that of radiolabeled nanoparticles, which is usually in the range of 3-6 %ID/cm^3 [27–29]. Albumin may be a vehicle for tumor accumulation of certain species such as radiometals or their hydroxides/oxides due to its metal binding capabilities [13]. Albumin has been labeled with ^{89}Zr through desferrioxamine and gave a biodistribution in tumor-bearing animals that was dominated by EPR-mediated tumor accumulation, with tumor values of 2-5 %ID/cm^3 measured until 20 h post injection [14]. While the level of tumor accumulation (2-4% ID/cm^3) observed in the present study is negligible with respect to signals observed with many highly specific mAbs (*eg.* J591-PSMA in LnCaP xenografts, 34-46 %ID/cm^3, [8]), it is not small compared to the uptakes expected in non-targeted nanoparticle imaging. Therefore, as ^{89}Zr becomes more prevalent in nanoparticle imaging, differentiating between the non-specific accumulation of free ^{89}Zr, versus that of the nanoparticles, must be taken into account.

As a further point, it should be noted that the impact of non-specific accumulation of free ^{89}Zr in spontaneous human cancers is unknown. If free ^{89}Zr exhibits tumor accumulation due to the EPR effect, translation from mice to humans may amplify the significance of non-specific uptake, especially in the case of imaging with ^{89}Zr-labeled mAbs. When imaging EPR-localizing agents, an increased tumor accumulation relative to total body mass from mice to humans is typically seen. Harrington et al. investigated ^{111}In-labeled liposomes and found tumor uptakes in mice ranging from 1-6 %ID/g over several days post-injection in an HNSCC-derived xenograft model [30]. In humans, they found a tumor uptake of 33 ± 16 %ID/kg at 72 hours [31]. On the contrary, targeted mAb imaging with U36 against HNX-OE (HNSCC-derived) xenografts in mice gave a striking uptake of 26±2 %ID/g at 144 hours[32], whereas the same mAb in humans with HNSCC had an average uptake of 19 %ID/kg[33]. From these data, it is apparent that uptake in man versus mouse is not directly scalable, but can depend on the mode of accumulation. Accordingly, we propose that if ^{89}Zr localizes to tumors by transferrin binding and EPR uptake, the impact on proper assessment of tumor uptake may be greater in humans when imaging antibodies that primarily localize by active targeting.

Finally, turning to the pulmonary aspergillosis model, the results illustrate that when imaging animals with advanced disease, the presence of free ^{89}Zr cannot be neglected. This disease model was expected to give an uptake of free ^{89}Zr that was significantly different from naïve animals for several reasons. First, as the disease progresses the lung tissue becomes highly perfused, thereby giving a higher PET signal due to blood volume in the ROI, and due to EPR

457 localization. Second, the inflammation in the lungs would lead to an upregulation of the Tf-
458 receptor causing accumulation of ^{89}Zr that might have been associated with transferrin *in vivo*.
459 And lastly, higher uptake was expected due to the presence of cyclic hydroxamate-based
460 chelates in the extracellular environment of the fungus. The results of the present study do not
461 weigh in on which of these probable causes are responsible, yet they do set a benchmark for
462 significance when attempting targeted approaches to pulmonary aspergillosis imaging.
463

464 ## 5 Conclusions

465

466 In this study we have shown that free ^{89}Zr, in the form of ^{89}Zr oxalate in saline, can exhibit
467 substantial tumor accumulation as well as significant accumulation in Aspergillus infected lungs
468 as compared to healthy lungs. Our results underline the importance of making sure that no free
469 ^{89}Zr is present when conducting ^{89}Zr PET imaging, especially in cancers and pulmonary
470 aspergillosis, as observed accumulation of radioactivity may be non-specific. In addition, our
471 results indicate that injection of free ^{89}Zr, preferably as an oxalate at pH < 7, should routinely be
472 performed as a control experiment to a preclinical study.
473

474 ## 6 Acknowledgements

475

476 This research was supported by the EU grant FP7 MATHIAS project, the Danish Cancer Society,
477 the Lundbeck Foundation, the Novo Nordisk Foundation, Innovationsfonden, the Svend
478 Andersen Foundation and the Arvid Nilsson Foundation.
479

7 References

[1] Vugts DJ, Visser GWM, van Dongen GAMS. ^{89}Zr-PET radiochemistry in the development and application of therapeutic monoclonal antibodies and other biologicals. Curr Top Med Chem 2013;13:446–57.

[2] Fischer G, Seibold U, Schirrmacher R, Wängler B, Wängler C. ^{89}Zr, a radiometal nuclide with high potential for molecular imaging with PET: chemistry, applications and remaining challenges. Molecules 2013;18:6469–90.

[3] Deri MA, Zeglis BM, Francesconi LC, Lewis JS. PET imaging with ^{89}Zr: From radiochemistry to the clinic. Nucl Med Biol 2013;40:3–14.

[4] Zhang Y, Hong H, Cai W. PET tracers based on zirconium-89. Curr Radiopharm 2011;4:131–9.

[5] Severin GW, Engle JW, Barnhart TE, Nickles RJ. ^{89}Zr radiochemistry for positron emission tomography. Med Chem 2011;7:389–94.

[6] Chang AJ, Desilva R, Jain S, Lears K, Rogers B, Lapi S. ^{89}Zr-radiolabeled trastuzumab imaging in orthotopic and metastatic breast tumors. Pharmaceuticals 2012;5:79–93.

[7] Van Rij CM, Sharkey RM, Goldenberg DM, Frielink C, Molkenboer JDM, Franssen GM, et al. Imaging of prostate cancer with immuno-PET and immuno-SPECT using a radiolabeled anti-EGP-1 monoclonal antibody. J Nucl Med 2011;52:1601–7.

[8] Holland JP, Divilov V, Bander NH, Smith-Jones PM, Larson SM, Lewis JS. ^{89}Zr-DFO-J591 for immunoPET of prostate-specific membrane antigen expression in vivo. J Nucl Med 2010;51:1293–300.

[9] Abou DS, Ku T, Smith-Jones PM. In vivo biodistribution and accumulation of ^{89}Zr in mice. Nucl Med Biol 2011;38:675–81.

[10] Weiner R. The mechanism of ^{67}Ga localization in malignant disease. Nucl Med Biol 1996;23:745–51.

[11] Jørgensen JT, Persson M, Madsen J, Kjær A. High tumor uptake of ^{64}Cu: implications for molecular imaging of tumor characteristics with copper-based PET tracers. Nucl Med Biol 2013;40:345–50.

[12] Sotogaku N, Endo K, Hirunuma R, Enomoto S, Ambe S, Ambe F. Biochemical reactions of various trace elements with blood components and transport proteins. J Radioanal Nucl Chem 1999;239:429–32.

[13] Bal W, Sokołowska M, Kurowska E, Faller P. Binding of transition metal ions to albumin: sites, affinities and rates. Biochim Biophys Acta 2013;1830:5444–55.

[14] Heneweer C, Holland JP, Divilov V, Carlin S, Lewis JS. Magnitude of enhanced permeability and retention effect in tumors with different phenotypes: ^{89}Zr-albumin as a model system. J Nucl Med 2011;52:625–33.

[15] Matsumura Y, Maeda H. A new concept for macromolecular therapeutics in cancer chemotherapy: Mechanism of tumoritropic accumulation of proteins and the antitumor agent Smancs. Cancer Res 1986;46:6387–92.

[16] Schrettl M, Bignell E, Kragl C, Sabiha Y, Loss O, Eisendle M, et al. Distinct roles for intra- and extracellular siderophores during Aspergillus fumigatus infection. PLoS Pathog 2007;3:1195–207.

[17] Petrik M, Haas H, Dobrozemsky G, Lass-Flörl C, Helbok A, Blatzer M, et al. ^{68}Ga-siderophores for PET imaging of invasive pulmonary aspergillosis: proof of principle. J Nucl Med 2010;51:639–45.

[18] Petrik M, Franssen GM, Haas H, Laverman P, Hörtnagl C, Schrettl M, et al. Preclinical evaluation of two ^{68}Ga-siderophores as potential radiopharmaceuticals for Aspergillus fumigatus infection imaging. Eur J Nucl Med Mol Imaging 2012;39:1175–83.

[19] Chiani M, Akbarzadeh A. Production of desferrioxamine B (Desferal) using corn steep liquor in Streptomyces pilosus. Pak J Biol Sci 2010;13:1151–5.

[20] Holland JP, Sheh Y, Lewis JS. Standardized methods for the production of high specific-activity zirconium-89. Nucl Med Biol 2009;36:729–39.

[21] Bruns S, Kniemeyer O, Hasenberg M, Aimanianda V, Nietzsche S, Thywissen A, et al. Production of extracellular traps against Aspergillus fumigatus in vitro and in infected lung tissue is dependent on invading neutrophils and influenced by hydrophobin RodA. PLoS Pathog 2010;6:e1000873.

[22] Kobayashi T, Sasaki T, Takagi I, Moriyama H. Zirconium solubility in ternary aqueous system of Zr(IV)-OH-carboxylates. J Nucl Sci Technol 2009;46:142–8.

[23] Guérard F, Lee Y-S, Tripier R, Szajek LP, Deschamps JR, Brechbiel MW. Investigation of Zr(IV) and ^{89}Zr(IV) complexation with hydroxamates: Progress towards designing a better chelator than desferrioxamine B for immuno-PET imaging. Chem Commun 2013;49:1002–4.

[24] Holland JP, Evans MJ, Rice SL, Wongvipat J, Sawyers CL, Lewis JS. Annotating MYC status with ^{89}Zr-transferrin imaging. Nat Med 2012;18:1586–91.

[25] Gotthardt M, Bleeker-Rovers CP, Boerman OC, Oyen WJG. Imaging of inflammation by PET, conventional scintigraphy, and other imaging techniques. J Nucl Med Technol 2013;41:157–69.

[26] Vavere AL, Welch MJ. Preparation, biodistribution, and small animal PET of ^{45}Ti-transferrin. J Nucl Med 2005;46:683–90.

[27] Jensen AI, Binderup T, Kumar EK P, Kjær A, Rasmussen PH, Andresen TL. Positron emission tomography based analysis of long-circulating cross-linked triblock polymeric micelles in a U87MG mouse xenograft model and comparison of DOTA and CB-TE2A as chelators of copper-64. Biomacromolecules 2014;15:1625–33.

[28] Petersen AL, Binderup T, Rasmussen P, Henriksen JR, Elema DR, Kjær A, et al. ^{64}Cu loaded liposomes as positron emission tomography imaging agents. Biomaterials 2011;32:2334–41.

[29] Abou DS, Thorek DLJ, Ramos NN, Pinkse MWH, Wolterbeek HT, Carlin SD, et al. ^{89}Zr-labeled paramagnetic octreotide-liposomes for PET-MR imaging of cancer. Pharm Res 2013;30:878–88.

[30] Harrington KJ, Syrigos KN, Uster PS, Abra RM, Stewart JSW. Biodistribution and pharmacokinetics of In-DTPA-labelled pegylated liposomes in a human tumour xenograft model : implications for novel targeting strategies. Br J Cancer 2000;83:232–8.

[31] Harrington KJ, Mohammadtaghi S, Uster PS, Harrington KJ, Mohammadtaghi S, Uster PS, et al. Effective targeting of solid tumors in patients with locally advanced cancers by radiolabeled pegylated liposomes effective targeting of solid tumors in patients with locally advanced cancers by radiolabeled pegylated liposomes. Clin Cancer Res 2001:243–54.

[32] Verel I, Visser GWM, van Dongen GAMS. The promise of immuno-PET in radioimmunotherapy. J Nucl Med 2005;46 Suppl 1:164S–71S.

[33] Börjesson PKE, Jauw YWS, de Bree R, Roos JC, Castelijns JA, Leemans CR, et al. Radiation dosimetry of ^{89}Zr-labeled chimeric monoclonal antibody U36 as used for immuno-PET in head and neck cancer patients. J Nucl Med 2009;50:1828–36.

Table 1. pH ranges of ^{89}Zr complex preparations as measured after 10 minutes of mixing of ^{89}Zr chloride with the corresponding solution.

Mixture	pH range
Oxalate 5.5	4.87 – 6.01
Oxalate 7.0	6.74 – 7.45
Citrate 5.5	5.43 – 5.58
Citrate 7.0	6.60 – 6.93
Sucrose	5.12 – 6.77
Acetate 5.5	5.51 – 5.52
Acetate 7.0	6.43 – 7.54
Chloride	4.99 – 5.68
Water	4.65 – 4.95

Table 2. Biodistribution of ^{89}Zr, injected as the oxalate, in tumor-bearing mice. Averages and standard deviations are given (n = 3 for FaDu, n = 4 for HT29). Animals were injected intravenously with ^{89}Zr oxalate and imaged for up to 68 h. Tumor levels were higher than muscle at all measurement points. Tumor levels were higher than blood (heart) after 45 h. Errors indicate one standard deviation. 9-15 MBq was administered to each mouse, 10 min scans were acquired

		%ID/g (± SD)						
	Xenograft	**Heart**	**Kidney**	**Bladder**	**Liver**	**Tumor**	**Muscle**	**Bone**
	All (n = 7)	**10.59 (± 2.47)**	**4.69 (± 1.21)**	**4.04 (± 2.91)**	**6.07 (± 1.92)**	**2.99 (± 0.35)**	**1.98 (± 0.31)**	**4.30 (± 1.08)**
1h	FaDu	11.83 (± 3.01)	5.55 (± 1.45)	2.93 (± 1.00)	7.40 (± 2.26)	2.97 (± 0.37)	2.03 (± 0.42)	4.53 (± 1.66)
	HT29	9.65 (± 1.84)	4.05 (± 0.48)	4.88(± 3.76)	5.08 (± 0.93)	3.00 (± 0.36)	1.94 (± 0.26)	4.13 (± 0.64)

	All (n = 7)	**5.31 (± 2.42)**	**2.56 (± 1.09)**	**3.26 (± 0.91)**	**3.36 (± 1.69)**	**3.46 (± 0.65)**	**1.76 (± 0.46)**	**9.04 (± 2.59)**
6h	FaDu	6.53 (± 2.95)	3.25 (± 1.31)	3.23 (± 1.46)	4.37 (± 2.02)	4.08 (± 0.41)	2.05 (± 0.55)	10.37 (± 3.58)
	HT29	4.40 (± 1.81)	2.04 (± 0.61)	3.28 (± 0.48)	2.60 (± 1.09)	2.99 (± 0.29)	1.54 (± 0.25)	8.05 (± 1.35)
	All (n = 7)	**1.86 (± 1.49)**	**1.35 (± 0.68)**	**1.05 (± 0.28)**	**1.77 (± 1.33)**	**2.99 (± 1.22)**	**0.99 (± 0.40)**	**12.76 (± 2.24)**
20h	FaDu	3.07 (± 1.47)	1.85 (± 0.77)	1.15 (± 0.34)	2.77 (± 1.46)	4.13 (± 0.96)	1.37 (± 0.23)	13.63 (± 1.56)
	HT29	0.95 (± 0.65)	0.97 (± 0.31)	0.97 (± 0.25)	1.03 (± 0.60)	2.14 (± 0.40)	0.71 (± 0.18)	12.10 (± 2.65)
	All (n = 7)	**0.67 (± 0.56)**	**0.91 (± 0.44)**	**0.60 (± 0.22)**	**1.39 (± 0.99)**	**2.47 (± 0.95)**	**0.76 (± 0.36)**	**14.89 (± 1.32)**
45h	FaDu	1.09 (± 0.67)	1.24 (± 0.53)	0.72 (± 0.32)	2.14 (± 1.19)	3.27 (± 0.97)	1.07 (±) 0.36	13.17 (± 0.78)
	HT29	0.35 (± 0.09)	0.66 (± 0.10)	0.50 (± 0.04)	0.83 (± 0.26)	1.88 (± 0.23)	0.53 (± 0.10)	15.58 (± 1.25)
	All (n = 7)	**0.55 (± 0.31)**	**0.86 (± 0.32)**	**0.50 (± 0.08)**	**1.30 (± 0.82)**	**2.05 (± 0.76)**	**0.65 (± 0.29)**	**12.99 (± 1.45)**
68h	FaDu	0.86 (± 0.14)	1.00 (± 0.40)	0.54 (± 0.08)	1.93 (± 0.92)	2.72 (± 0.74)	0.78 (± 0.37)	13.77 (± 0.32)
	HT29	0.32 (± 0.06)	0.75 (± 0.24)	0.48 (± 0.07)	0.82 (± 0.27)	1.55 (± 0.13)	0.56 (± 0.20)	12.41 (± 1.75)

Table 3. *Ex vivo* biodistribution of organs of naïve (n = 4) and infected mice (n = 4). The mice were infected with *A. fumigatus* and after 21 hours of disease progression, they were injected with 10-12 MBq ^{89}Zr oxalate. Tissues were excised and measured three hours after the injection. Data are %ID/g, expressed as the mean or as lung-to-muscle ratios ± 1 SD. Significantly different organs are shown in bold with * ($p < 0.05$) or ** ($p < 0.01$).

Organ	Näive mice	Infected mice
Blood	10.5 (± 2.7)	8.6 (± 2.8)
Lung**	**6.0 (± 1.1)**	**11.6 (± 1.8)**
Muscle	1.6 (± 0.5)	1.9 (± 0.2)
Liver	4.0 (± 0.8)	3.3 (± 0.7)
Heart	5.8 (± 2.2)	5.6 (± 1.5)
Kidney	6.1 (± 1.5)	8.3 (± 1.6)

Stomach*	**2.5 (± 0.2)**	**3.5 (± 0.7)**
Colon*	**2.6 (± 0.4)**	**3.5 (± 0.2)**
Brain	0.5 (± 0.1)	0.5 (± 0.1)
Spine*	**5.0 (± 0.9)**	**3.8 (± 0.4)**
Femur right	9.9 (± 4.3)	6.6 (± 0.5)
Femur left	9.0 (± 3.5)	6.5 (± 1.3)
Lung/muscle	3.8 (± 2.3)	6.3 (± 7.7)

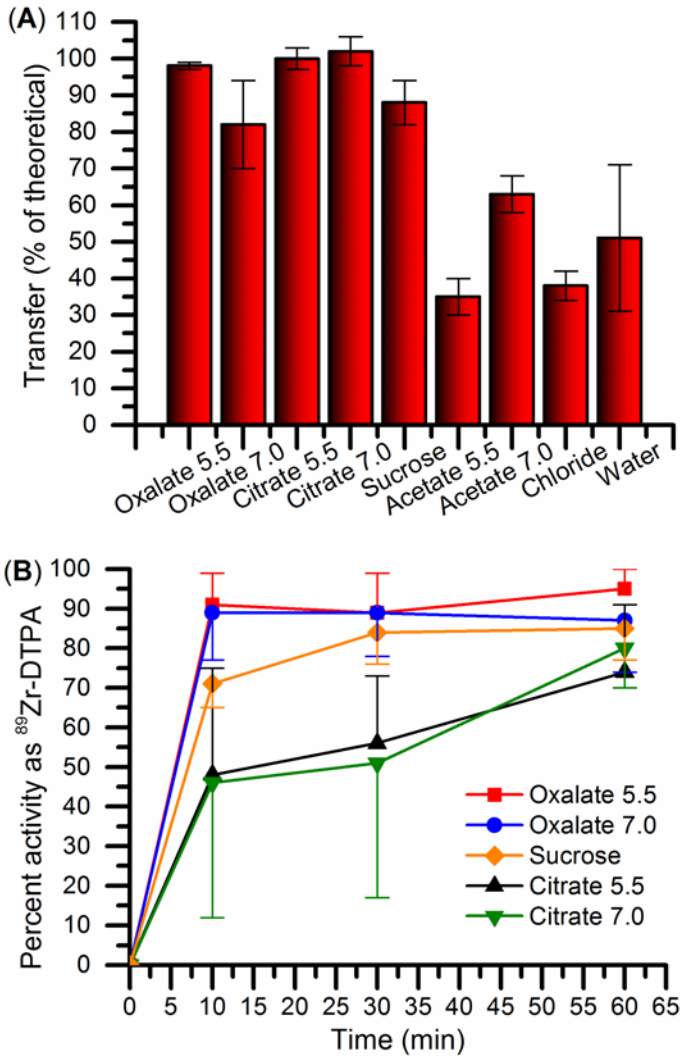

Figure 1. (**A**) Transferability/dissolution of ^{89}Zr mixtures. The y-axis shows transferability as the activity in a removed aliquot of 300 µL compared to the theoretical maximum activity removed from a homogeneous solution, as calculated by the equation *transferability* = $A_{300\mu L}$*(1.3/0.3) / $A_{1300\mu L}$ * *100%*. n = 3 in all cases, error bars show one standard deviation. (**B**) Transchelation of ^{89}Zr mixtures to DTPA. Oxalate at both pH values showed fast transchelation, reaching about 90% after 10 minutes, while sucrose and especially the citrates showed a slower shift of the radioactivity to DTPA. n = 3 in all cases, error bars showing one standard deviation are one-sided to improve legibility.

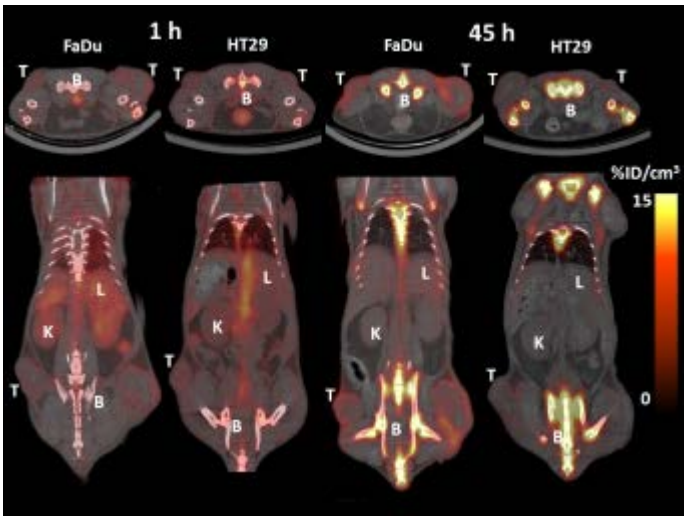

Figure 2. Representative transverse (top lane) and coronal (bottom lane) images of ^{89}Zr-distribution in FaDu and HT29 tumor bearing animals acquired by ten minute static PET scans, 1 h (left) and 45 h (right) after tracer administration (FaDu: 12.47 MBq injected, HT29: 9.40 MBq injected). Animals were sedated with sevoflurane. White letters on images marks T: tumor; B: bone; L: liver and K: kidney.

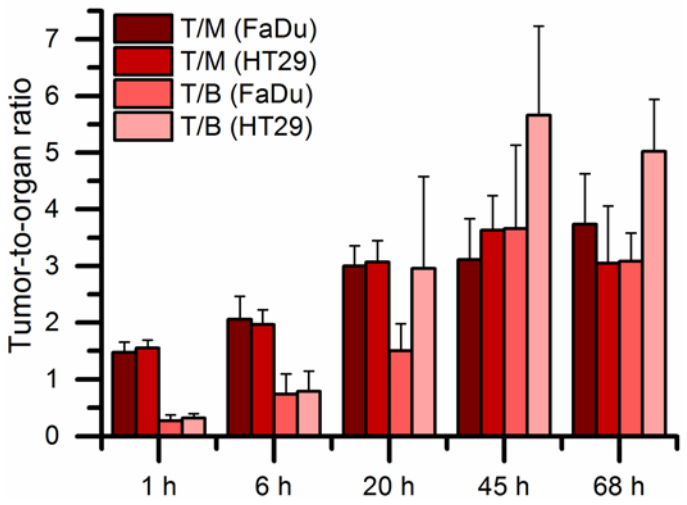

Figure 3. Tumor-to-muscle (T/M) and tumor-to-blood (T/B) ratios of injected ^{89}Zr oxalate in mice bearing FaDu or HT29 tumor xenografts. The blood values are taken as %ID/cm^3 of the heart. The T/M values for both tumor types are seen to rise until 20 h and subsequently stabilize

between 3.0-3.7 for both tumors. T/B values for both tumor types increase until 45 h. Error bars indicate one standard deviation. n = 3 (FaDu), n = 4 (HT29). 9-15 MBq was administered to each mouse, 10 min scans were acquired.

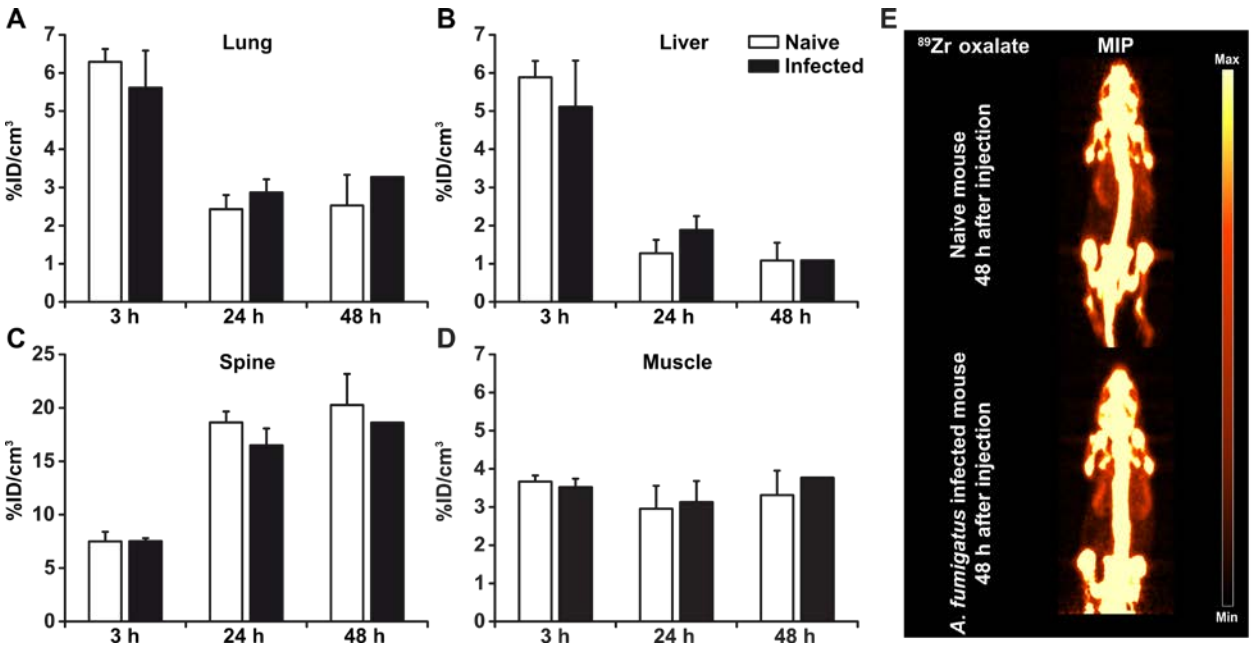

Figure 4 (A)-(D). PET quantification (%ID/cm^3) of organs of naïve and infected mice 3 h, 24 h, 48 h post injection of ^{89}Zr oxalate. **(E)** Maximum intensity projection (MIP) of a naïve and an infected mouse at the 48 h time-point, demonstrating the high uptake of ^{89}Zr in the bones. Injected radioactivity was between 10 and 12 MBq. The mice were sedated with isoflurane and scanned for 10 minutes. Data are given as %ID/cm^3 ± 1 SD.

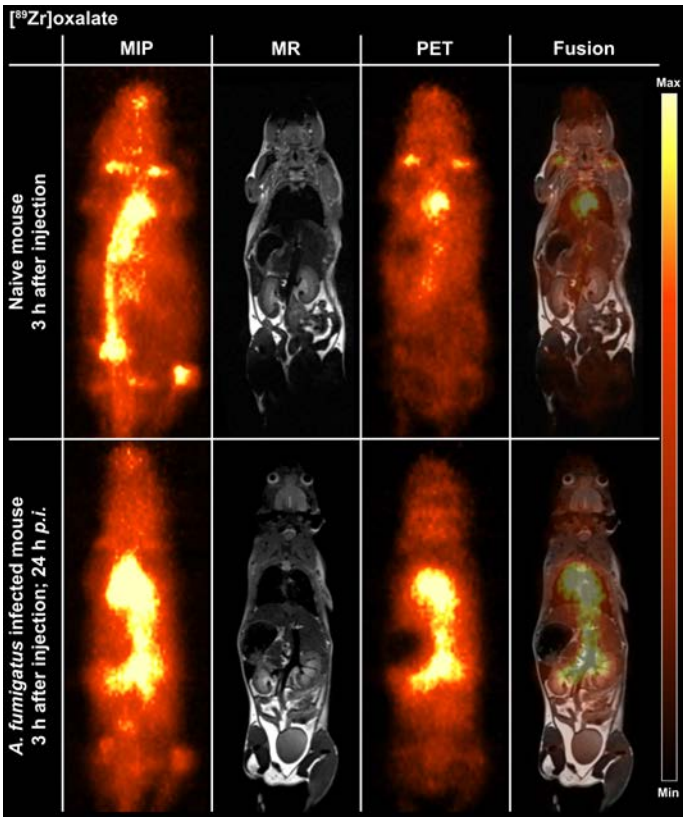

Figure 5. Maximum intensity projections (MIP) of PET and fused PET and MR images of naïve or neutropenic *A. fumigatus* infected mice. The PET/MR imaging was done three hours after injection with ^{89}Zr oxalate and 21 hours post infection (p.i.) of the mice with *A. fumigatus*. Perfusion effects and thereby enhanced ^{89}Zr oxalate accumulation is seen in the lungs of the *A. fumigatus* infected mouse as depicted in the lower lane. The mice were sedated with isoflurane and scanned for 10 minutes. Injected radioactivity was between 10 and 12 MBq

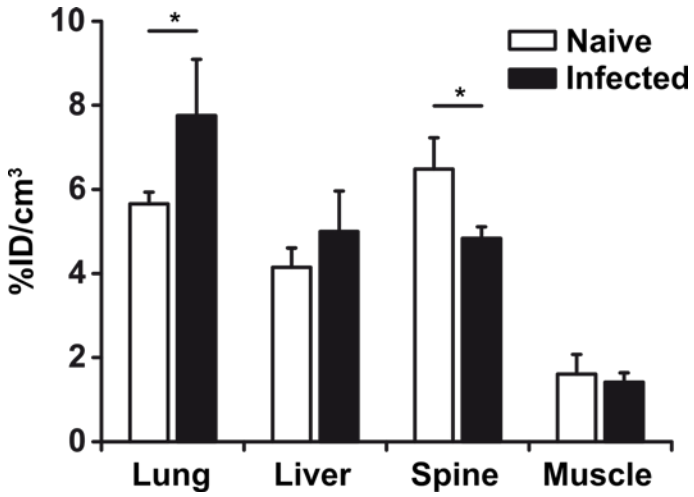

Figure 6. PET quantification (%ID/cm^3) of tissue ROIs from naïve and infected mice with advanced disease. The data were taken 24 h post-infection, and 3 h after injection of ^{89}Zr oxalate. Data are given as %ID/cm^3 ± 1 SD. *Tissues are considered statistically significant, with $p<0.05$.